Hue University Journal of Science: Natural Science
Vol. 132, No. 1B, 65–72, 2023

pISSN 1859-1388
eISSN 2615-9678

Synthesis and Investigation of Physical Properties of Multiferroic $BaDyFeO_4$

Le Thi Phuong Thao[1,2], Danh Bich Do[3], Dinh Thanh Khan[2], Tran Tuan Anh[4], Le Vu Truong Son[2], Dang Ngoc Toan[5], Nguyen Truong-Tho[1]*

[1] Faculty of Electronics, Electrical Engineering and Material Technology, University of Sciences, Hue University, 530000 Hue, Vietnam
[2] University of Science and Education, The University of Danang, 550000 Danang, Vietnam
[3] Faculty of Physics, Hanoi National University of Education, 100000 Hanoi, Vietnam
[4] Ho Chi Minh City University of Technology and Education, 700000 Ho Chi Minh, Vietnam
[5] Institute of Research and Development, Duy Tan University, 550000 Danang, Vietnam

* Correspondence to Nguyen Truong Tho <ntthokh@hueuni.edu.vn>

(*Received: 24 September 2022; Accepted: 06 December 2022*)

Abstract. Materials exhibiting magnetoelectric effects have drawn great interest because of their intriguing physical phenomena and potential applications in electronic devices. The magnetoelectric (ME) coupling makes them promising for use in multifunctional devices with electric-field-tunable magnetism and magnetic-field-controlled ferroelectricity. Very recently, a strong ME effect has been found in the $BaRFeO_4$ system (R is a rare-earth element), in which the ferroelectricity is driven by the onset of a long-range cycloidal antiferromagnetic order of Fe spins. However, previous studies have shown how complicated the synthesis procedure is for obtaining single-phase samples of the materials. In this work, we present a simple and easy fabrication process to synthesize high-quality $BaDyFeO_4$ using the conventional solid-state reaction method. The structural, morphological, and optical properties of the synthesized sample have been investigated by means of X-ray diffraction, scanning electron microscopy, and UV-Vis spectroscopy, respectively. It is found that the sample is formed from high-quality microparticles. The X-ray diffraction study has revealed the single-phase nature of the sample, adopting the *Pnma* orthorhombic structure without any impurity phases. The detailed structural parameters have been refined by the Rietveld refinement. The sample demonstrates direct-gap semiconducting behavior. The experimental results of the structural and electronic properties of $BaDyFeO_4$ are complemented by density functional theory (DFT) calculations.

Keywords: multiferroics; synthetic procedure; crystal structure; semiconductor; DFT calculation

1 Introduction

Multiferroics are materials that simultaneously possess ferroelectric and magnetic orders. It is worth noting that the most interesting and useful property of multiferroics is the magnetoelectric coupling, which facilitates direct control of magnetic properties electrically and vice versa. This makes these materials promising candidates for practical applications in multifunctional devices such as sensitive electromagnetic sensor designs, fast transducers, ferromagnetic resonance devices controlled by an electric field, electrically tunable microwave devices, multiple state memory elements, DRAM, MRAMs, FeRAMs, and RRAM …(1,2). More importantly, the simultaneous coexistence of several ordered states in the same material phase can reduce the size, increase the density, and speed up the performance of the components of the multifunctional devices (1,2).

Generally, multiferroics can be divided into two main groups: geometric and spin-driven. The geometric multiferroics like $BiFeO_3$ and hexagonal $RMnO_3$ (R - rare-earth elements) are characterized by ferroelectric transition temperatures significantly exceeding magnetic ordering ones and relatively weak coupling of relevant order parameters. It is due to the different origins of ferroelectricity and magnetism (3, 4). For instance, ferroelectricity requires the presence of a transition metal with an empty d^0 configuration or lone electron pairs of Bi^{3+} and Pb^{2+} (3), whereas magnetism requires partially filled *d*-orbitals on the same site. As a result, strong magnetoelectric coupling is not expected in multiferroics with geometric ferroelectricity (5).

On the other hand, spin-driven multiferroics, where ferroelectricity is induced by the formation of complex antiferromagnetic ordering, are characterized by a strong magnetoelectric coupling and lose ferroelectric and magnetic ordering temperatures (6, 7). It is worth noting that spin-induced ferroelectricity is commonly observed in magnetically frustrated systems, since spin frustration induces spatial variation in magnetization, which leads to the loss of the lattice inversion symmetry, thereby resulting in the occurrence of ferroelectricity (6, 7). Recently, $BaYFeO_4$ has been reported to exhibit the spin-driven ferroelectricity along with unusual magnetic properties, including the coexistence of the cycloidal long-range magnetic order and a spin-cluster glass state (8,9). The phenomena were proposed to originate from the strong geometric magnetic frustration due to their peculiar crystal structure c. Interestingly, $BaDyFeO_4$ has recently been reported to exhibit magnetic and dielectric properties distinctive from those of $BaYFeO_4$ (8,9). Moreover, no ferroelectric phase was detected in $BaDyFeO_4$ (8,9). The nature of the magnetic and ferroelectric properties of the compound remains unclear. One important point should be noted : the presence of impurities strongly affects the physical properties of compounds (8,10). Furthermore, Belik et al. showed that it was impossible to obtain a single-phase sample of $BaDyFeO_4$, despite using a very complex fabrication procedure (8). The successful fabrication of multiferroics is an important first step to further studying their properties. In this article, we show a simpler and easier fabrication process to fabricate pure and single-phase $BaDyFeO_4$.

2 Experimental and DFT calculation details

The $BaDyFeO_4$ sample was prepared from stoichiometric mixtures of $BaCO_3$, Dy_2O_3, and Fe_2O_3 (purities 99.9%) by the solid-state reaction method. To remove possible adsorption water, all precursors were dried at 250°C for 2 hours before weighing by the following equation:

$$½\ Dy_2O_3 + ½\ Fe_2O_3 + BaCO_3 \rightarrow BaDyFeO_4 + CO_2.$$

The mixtures were ground, pressed into a pellet, and annealed in the air on an Al_2O_3 crucible at 900°C for 12 hours. After the first annealing, the sample was calcined several times at 1250°C for 24 hours, with grinding and pellet pressing after each step.

The crystal structure of the sample was characterized by an X-ray diffractometer D8 Advance Eco (Bruker) equipped with a Cu-Kα radiation source (λ = 1.54056 Å). X-ray diffraction (XRD) data were recorded in the angle range 2θ = 20 - 80° with the scanning step and scanning speed fixed at 0.01° and 1°/min, respectively. The XRD data were analyzed by the Rietveld method using the Fullprof program (11).

The morphological properties and chemical compositions of synthesized $BaDyFeO_4$ were analyzed using a scanning electron microscope equipped with energy dispersive X-ray (JSM-

pISSN 1859-1388
eISSN 2615-9678

IT200, JOEL, Horiba). The absorption spectrometry was measured using a Jasco 670 UV spectrometer.

In order to explain the results obtained from the experiment, we performed DFT calculations based on the structural parameters obtained from the XRD data. First-principle DFT calculations for the $BaDyFeO_4$ compound were performed using the Quantum ESPRESSO package (12,13), with the generalized gradient approximation in the parameterization of Perdew, Burke and Enzerhof (PBE) (14,15). A projector augmented wave method (PAW) was used, and 5*s*5*p*6*s* of Ba, 4*d*4*f*5*s*5*p*6*s* of Dy, 3*d*4*s* of Fe, and 2*s*2*p* of O were treated as valence electrons. We applied Hubbard U terms (16) with different values of U for Fe to account for strong electronic correlations, and the value U of 8.2eV, at which the difference between experiment and calculation is minimum, was chosen for all calculations. We used a 56-atom unit cell for the $BaDyFeO_4$ compound. A cutoff energy of 800 Ry and a Monkhorst-Pack special *k*-point mesh of 3×6×4 for the Brillouin zone integration were found to be sufficient to obtain convergence (17). Self-consistent iterations finish when the difference in total energy between two steps is less than 10^{-6} Ry. The cell optimizations stop when the force of each atom between two steps is less than 10^{-5} Ry/Bohr.

3 Results and discussion

The XRD patterns of $BaDyFeO_4$ after calcinations are shown in Fig. 1. As can be seen in Fig. 1, after the first calcination, the relative intensity of the XRD peaks gradually stabilized, and the noise peaks gradually decreased in intensity. Upon further calcinations, the main features of the diffraction pattern remain almost unchanged, reflecting the stability of the sintered phase. Further, the data analysis has shown that the characteristic diffraction peaks correspond to the orthorhombic structural phase of $BaDyFeO_4$ with *Pnma* symmetry and lattice parameters of $a \approx 13.16$ Å, $b \approx 5.71$ Å, and $c \approx 10.26$ Å. Furthermore, the Rietveld refinement of the XRD data (Fig. 2) within the *Pnma* structural model also provided a satisfactory fit, confirming again the formation of the expected phase of $BaDyFeO_4$. However, by a close inspection, it can be seen that there are two unindexed, relatively weak peaks located at the 2θ positions of 29.05° and 30.82° in the XRD pattern after the first calcination (see Figs. 1 and 2), reflecting the presence of impurity phases. These peaks completely disappeared after the second calcination, evidencing the full suppression of the impurity phases. The single-phase nature of the synthesized samples has been confirmed by the Rietveld refinement of the XRD patterns (Fig. 2).

As an important result of the structural refinement, the lattice parameters and atomic positions of the synthesized $BaDyFeO_4$ are refined and listed in Table 1. The obtained results are consistent with those previous studies (8). As shown in Fig. 3, in the orthorhombic crystal structure of $BaDyFeO_4$ there are two independent crystallographic sites for Fe ions; Fe1 and Fe2, which are surrounded by oxygen octahedra and pyramids, respectively. In the $Fe1O_6$ octahedra, the Fe atom is surrounded by 6 O atoms with bond lengths ranging from 1.959 to 2.101 Å. The $Fe2O_5$ pyramids contain Fe in the center and 5 O atoms surrounding Fe, with Fe-O bond lengths ranging from 1.856 to 2.045 Å. The $Fe1O_6$ octahedra are linked to the $Fe2O_5$ pyramids through common vertices, forming Fe_4O_{18} rings. The Fe_4O_{18} rings stack and bond to each other through common edges in order to form a two-dimensional column along the *b* crystal axis (Fig. 3).

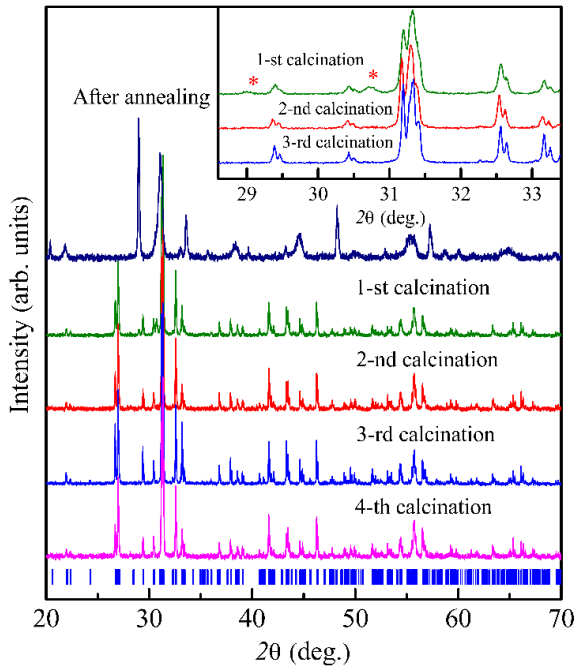

Fig. 1. XRD patterns of the synthesized $BaDyFeO_4$ samples at different synthesis stages. The ticks below represent calculated positions of the nuclear peaks of the Pnma orthorhombic structural phase of $BaDyFeO_4$. The inset illustrates an enlarged part of the XRD patterns

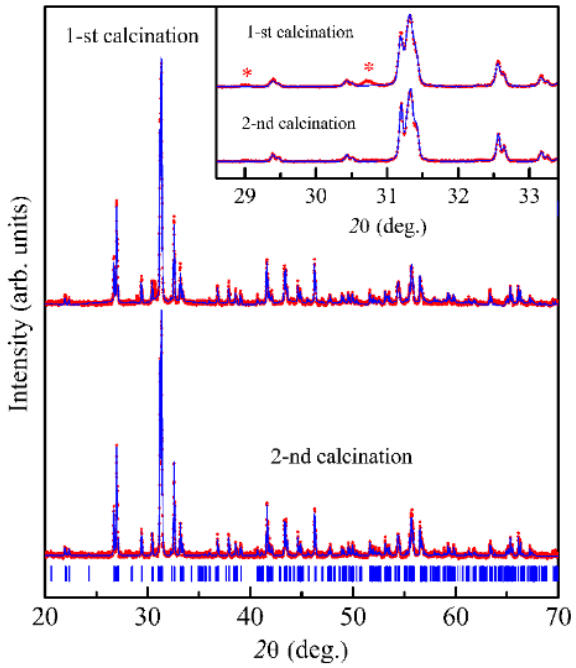

Fig. 2. XRD diffraction patterns of $BaDyFeO_4$ after the first and second calcinations, refined by the Rietveld method. The experimental points (red color) and calculated profiles (blue lines) are shown. The ticks below represent calculated positions of the nuclear peaks of the Pnma orthorhombic structural phase. The symbol "*" denoted the peaks of impurity phases

Table 1. Structural parameters of the orthorhombic crystal phase of $BaDyFeO_4$ refined from the room temperature XRD data refinement. Space group *Pnma*, a = 13.1669(3) Å, b = 5.7089(2) Å, and c = 10.2663(2) Å.

Atom	Site	*x*	*y*	*z*
Ba1	4c	0.214(2)	0.250	0.672(3)
Ba2	4*c*	0.418(3)	0.250	0.395(3)
Dy1	4*c*	0.414(3)	0.250	0.016(2)
Dy2	4*c*	0.141(2)	0.250	0.308(3)
Fe1	4*c*	0.467(4)	0.250	0.708(3)
Fe2	4*c*	0.184(4)	0.250	0.0299(3)
O1	4*c*	0.593(8)	0.250	0.612(7)
O2	4*c*	0.297(8)	0.250	0.197(9)
O3	8*d*	0.001(8)	0.509(8)	0.365(9)
O4	8*d*	0.227(9)	0.488(8)	0.441(9)
O5	8*d*	0.089(9)	0.997(7)	0.114(7)

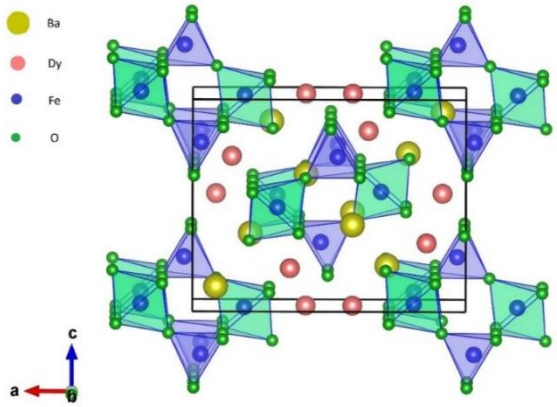

Fig. 3. BaDyFeO4 crystal structure

In the $BaDyFeO_4$ crystal, Dy atoms are located at the space between the Fe_4O_{18} rings. The distance between them and the nearest atom is 2.230 Å, corresponding to the Dy1-O3 bond, while the distance to the farthest atom is 3.156 Å, corresponding to the Dy1–Fe1 bond. Compared

pISSN 1859-1388
eISSN 2615-9678

with the $BaYFeO_4$ structure (17), these distances are different due to the difference in the radii of ions Y and Dy. In view of the role of the rare earth element R in the magnetic interaction between Fe^{3+} ions (8,9), this difference may be the main cause of the difference in the magnetic properties of $BaYFeO_4$ and $BaDyFeO_4$.

Further, the particle morphology of the $BaDyFeO_4$ material was checked by a scanning electron microscope. The SEM image is shown in Fig. 4(a). The image shows that the sample consists of cylinder-shaped particles. Most particles are about 2-3 μm in size. Others have an outstanding size of around 8-9 μm. The particle sizes are counted and shown in Fig. 4(b). Furthermore, the density of the synthesized $BaDyFeO_4$ measured through a methanol solution is d_{exp} = 5.71 g/cm³. On the other hand, with the unit-cell values obtained from the XRD data refinement, we could calculate the X-ray density (d_x) from the equation $d_x = nM_0/N_AV$, in which n is the number of molecules per unit cell, M_0 is the molecular weight, N_A is Avogadro's number, and V is the unit-cell volume (11). The d_x value calculated from the lattice parameters is about 7.225 g/cm³, which is higher than the d_{exp} value. The difference implies the presence of porosity of about 20%, evidenced by the observation of micro-sized chinks between microparticles from the SEM image (Fig. 4a).

In order to check the distribution of the elemental composition in the sample, the X-ray energy dispersive spectrum of $BaDyFeO_4$ was collected at various points of the sample. Fig. 5 shows a typical X-ray energy dispersive spectrum of $BaDyFeO_4$. The investigation showed that the elemental composition ratios at different points are quite similar and close to nominal concentrations (Fig. 5), implying the chemical homogeneity of the sample.

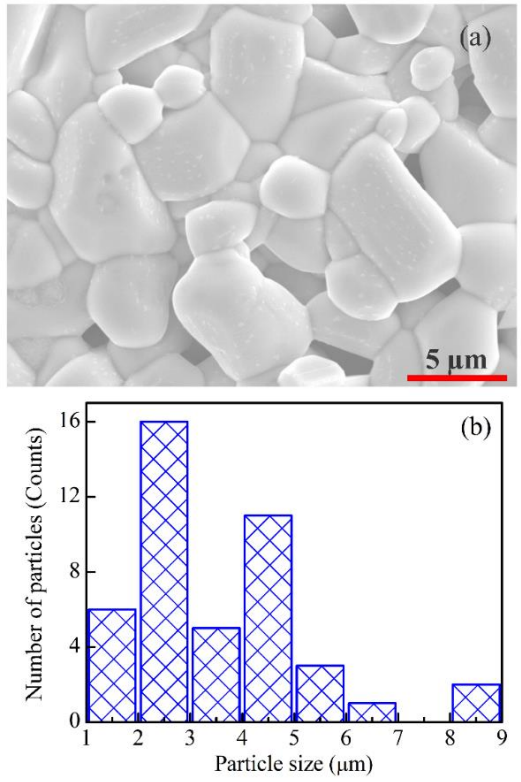

Fig. 4. (a) SEM micrograph and (b) particle size distribution of the $BaDyFeO_4$ sample.

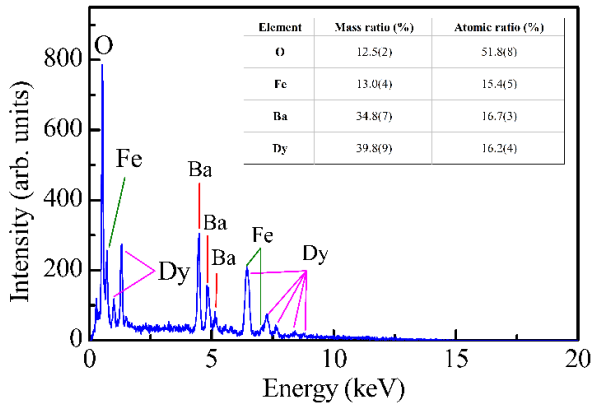

Fig. 5. X-ray energy dispersive spectrum of $BaDyFeO_4$

After assessing the crystal quality, the optical properties of $BaDyFeO_4$ were investigated through UV-visible absorption measurements. The absorption spectrum of the sample at room temperature is shown in Fig. 6. The sample presents a well-defined absorption edge, reflecting its semiconducting nature. The band gap energy can be estimated from the absorbance spectra using Tauc's method as follows: $(\alpha h\upsilon)^2$ =

$A(h\upsilon\text{-}E_g)$, where α is the absorption coefficient, $h\upsilon$ is the identical energy of the corresponding wavelength, A is a constant, and E_g is the band gap energy (18). We found that the band gap of $BaDyFeO_4$ is about 2.69 eV, which is close to that predicted from the DFT calculations shown below.

In order to explain the results obtained from the experiments, a DFT calculation was performed. In this work, we focus on the orthorhombic structure (space group *Pnma*) following the experimental results. We performed the structural relaxation of the $BaDyFeO_4$ system by the GGA+*U* method, regarding the influence of the parameter *U* on the ground-state structural parameters. The calculation results are listed in Table 2. We find the lattice *a* and *c* constants obtained within GGA+*U* show an increase, while the lattice constant *b* is slightly reduced. Correspondingly, the equilibrium volume increases with respect to U_{eff}, especially from *U* = 5 to 8.2 eV. The cell volume for *U* = 8.2 eV is 2.0% larger than that for *U* = 5 eV. The parameters of the crystal structure with *U* = 8.2 eV well agree with the experimental data (Table 2).

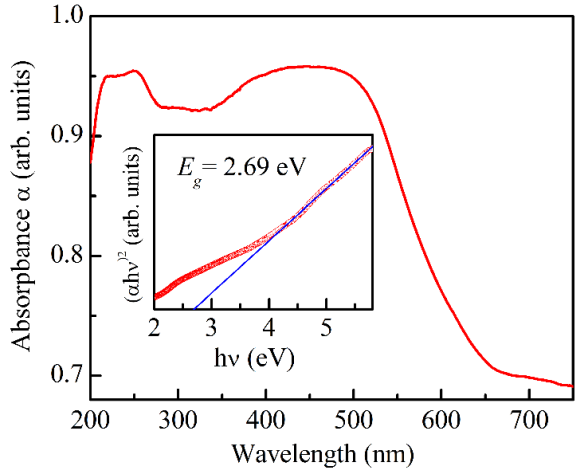

Fig. 6. The UV-Vis absorption spectrum of $BaDyFeO_4$. The inset shows the Tauc plot for the direct band gap of $BaDyFeO_4$.

Table 2. Comparison between experimental and DFT-calculated lattice parameters of $BaDyFeO_4$

	Experimental	**PBE+nonU**	**PBE+U= 5eV**	**PBE+U= 8.2eV**	a_{exp}-$a_{DFT(U=8.2eV)}$
a (Å)	13.1669	12.8932	12.9301	13.09476	0.56%
b (Å)	5.70890	5.6528	5.6794	5.6657	0.77%
c (Å)	10.2663	10.0888	10.0706	10.16431	1.01%
V (Å^3)	771.7025	735.2979	739.5358	754.0963	2.32%
Band gap (eV)	2.69	0.31	1.049	2.3	

Our calculation yields a direct bulk band gap of 2.3 eV for *U* = 8.2 eV, which is in good agreement with what has been experimentally observed above. The calculated band structure and partial density of states of $BaDyFeO_4$ are plotted in Fig. 7. The horizontal dash lines indicate the Fermi energy level. It is clearly observed that the top of the valence band (VB) and the bottom of the conducting band (CB) are located at the Gamma point. This band structure confirms the semiconducting behavior of the $BaDyFeO_4$ system. Due to the increase in the *U* value, the increase in the band gap is clearly seen. We also elucidated the features of the chemical bonds for $BaDyFeO_4$ on the basis of the total and angular momentum projected by DOS. According to Fig. 7b, the O 2*p* and Fe 3*d* states are the main contributors to the VBs ranging from the Fermi level to -4eV. In addition, the CBs between 2.3 and 2.6 eV are mostly formed by the states O 2p and Fe 3d. The Ba 5*p* and Dy 4*d* states only give rise to VBs. From the projected density of states (PDOS) plotted in Fig. 7, it can be observed that $BaDyFeO_4$

pISSN 1859-1388
eISSN 2615-9678

has inconsistent electronic distributions. Fe-*d* and O-*p* electrons dominate in the wide energy range and form strong covalent bonds, as suggested by the matching Fe-3*d* and O-2*p* curve shapes.

The electron localization function (ELF) can be viewed as a real-space indicator of the degree of electron localization. Thus, ELF serves to localize bonding and nonbonding electron pairs in the real space of the crystal structure. The ELF-density of $BaDyFeO_4$ at the plane (010) is shown in Fig. 8. The color bar on the chosen planes in Fig. 8 shows ELF density from 0 (at bottom blue color) to 1 (at top red color). The orange-red color around Fe and O atoms shows high electron density between Fe and O atoms, which again confirms the strong covalent Fe-O bonding within the three-dimensional Fe-O network (Fig. 8). As shown in figure 8, ELF shows two localization areas: one is located around Ba and the other around Dy atoms. Almost no electron is localized between Ba, Dy, and other atoms, suggesting typical ionic bonding, with Ba and Dy atoms donating electrons to O atoms.

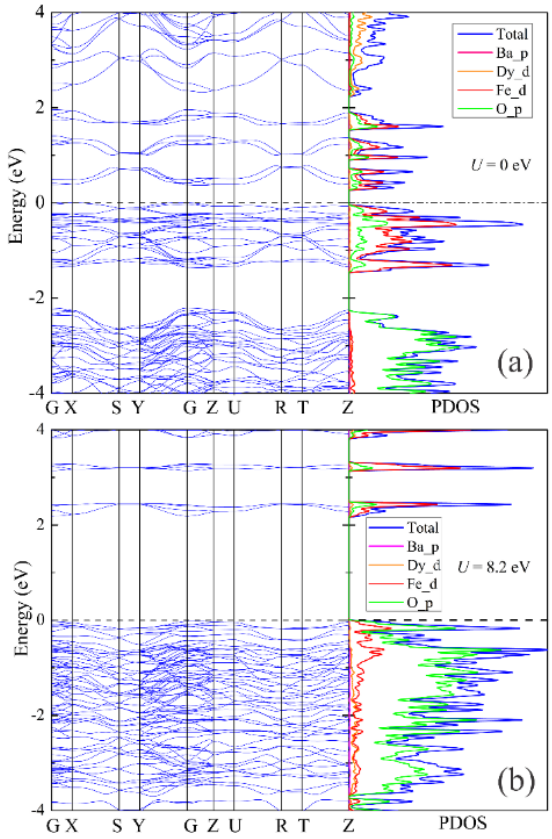

Fig. 7. Band structure and PDOS of $BaDyFeO_4$ with (a) U = 0 eV, (b) U = 8.2 eV

Fig. 8. Elf-density of $BaDyFeO_4$ at plane (010) across 4 Ba and 4 Dy atoms without (a) and with (b) atoms

4 Conclusions

We have successfully fabricated a single-phase $BaDyFeO_4$ material by the solid-phase reaction method with a simple and easy-to-follow fabrication process: one annealing in the air on an Al_2O_3 crucible at 900 °C for 12 h, two calcinations at 1250°C for 24 hours, with grinding and pellet-pressing after each step. The obtained sample is a single phase adopting the *Pnma* orthorhombic crystal structure. The synthesized sample consists of high-quality cylindrical microparticles and exhibits chemical homogeneity. It has been observed that the sample is a semiconductor with

a direct gap of E_g = 2.69 eV. The experimental results were confirmed by the DFT calculations.

Acknowledgment

The work was supported by the RFBR and VAST Grant No. 20-52-54002 and the Vietnam Ministry of Education and Training Grant No. B2022-SPK-07. Le Thi Phuong Thao was funded by Vingroup JSC and supported by the Master, PhD Scholarship Programme of Vingroup Innovation Foundation (VINIF), and the Institute of Big Data, code VINIF.2021.TS.043.

References

1. Chu YH, Martin LW, Holcomb MB, Gajek M, Han SJ, He Q, et al. Electric-field control of local ferromagnetism using a magnetoelectric multiferroic. Nat Mater. 2008;7(6):478-82.
2. Laukhin V, Skumryev V, Martí X, Hrabovsky D, Sánchez F, García-Cuenca MV, et al. Electric-field control of exchange bias in multiferroic epitaxial heterostructures. Phys Rev Lett. 2006;97(22):227201.
3. Van Den Brink J, Khomskii DI. Multiferroicity due to charge ordering. J Phys Condens Matter. 2008;20(43):434217.
4. Lorenz B, Wang YQ, Chu CW. Ferroelectricity in perovskite $HoMnO_3$ and $YMnO_3$. Phys Rev B. 2007;76(10):104405.
5. Fiebig M. Revival of the magnetoelectric effect. J Phys D Appl Phys. 2005;38(8):R123-52.
6. Fiebig M, Lottermoser T, Meier D, Trassin M. The evolution of multiferroics. Nat Rev Mater. 2016;1(8):16046.
7. Lawes G, Harris AB, Kimura T, Rogado N, Cava RJ, Aharony A, et al. Magnetically driven ferroelectric order in $Ni_3V_2O_8$. Phys Rev Lett. 2005;95(8):087205.
8. Belik AA, Terada N, Katsuya Y, Tanaka M, Glazkova IS, Sobolev AV, et al. Synthesis, structure, and magnetic and dielectric properties of magnetoelectric $BaDyFeO_4$ ferrite. J Alloys Compd. 2019;811:151963.
9. Glazkova IS, Belik AA, Sobolev A V., Smirnova MN, Ovanesyan NS, Presniakov IA. Modulated Magnetic Structures in $BaRFeO_4$ (R = Y and Dy): Magnetic and ^{57}Fe Mössbauer Investigations. J Phys Chem C. 2020;124(24):13374-84.
10. Ghara S, Sundaresan A. Coexistence of long-range cycloidal order and spin-cluster glass state in the multiferroic $BaYFeO_4$. J Phys Condens Matter. 2018 ;30(24):245802.
11. Rodríguez-Carvajal J. Recent advances in magnetic structure determination by neutron powder diffraction. Phys B. 1993;192(1-2):55-69.
12. Giannozzi P, Andreussi O, Brumme T, Bunau O, Buongiorno Nardelli M, Calandra M, et al. Advanced capabilities for materials modelling with Quantum ESPRESSO. J Phys Condens Matter. 2017;29(46):465901.
13. Giannozzi P, Baroni S, Bonini N, Calandra M, Car R, Cavazzoni C, et al. QUANTUM ESPRESSO: a modular and open-source software project for quantum simulations of materials. J Phys Condens Matter. 2009;21(39):395502.
14. Perdew JP, Wang Y. Accurate and simple density functional for the electronic exchange energy: Generalized gradient approximation. Phys Rev B. 1986;33(12):8800-2.
15. Perdew JP, Burke K, Ernzerhof M. Generalized Gradient Approximation Made Simple. Phys Rev Lett. 1996;77(18):3865-8.
16. Anisimov VI, Zaanen J, Andersen OK. Band theory and Mott insulators: Hubbard U instead of Stoner I. Phys Rev B. 1991;44(3):943-54.
17. Monkhorst HJ, Pack JD. Special points for Brillouin-zone integrations. Phys Rev B. 1976;13(12):5188-92.
18. Phong LTH, Dang NT, Dang NV, Nguyen V-Q, Manh DH, Nam PH, et al. Structural, optical and conductivity properties in tetragonal $BaTi_{1-x}Co_xO_3$ ($0 \leq x \leq 0.1$). RSC Adv. 2022;12(25):16119-30.